ACS OMEGA

Open Access

http://pubs.acs.org/journal/acsodf

Article

Synthesis, Structural, and Raman Investigation of Lanthanide Nitride Powders (*Ln* = La, Ce, Nd, Sm, Gd, Tb, Dy, Er, Lu)

Kiersten Kneisel,* Mohsen Maddah, Jay Chan, Ying Xu, Caitlin Casey-Stevens, Kiri Van Koughnet, William Holmes-Hewett, Harry Joseph Trodahl, and Franck Natali*

Cite This: *ACS Omega* 2024, 9, 47842−47847

Read Online

ACCESS | Metrics & More | Article Recommendations

ABSTRACT: Lanthanide nitride (*Ln*N) materials have garnered significant interest in recent years due to their promising potential as heterogeneous catalysts for green ammonia synthesis under low temperature and pressure reaction conditions. Here, we report on the synthesis of an extended series of lanthanide (*Ln*) nitride powders (*Ln* = lanthanum, cerium, neodymium, samarium, gadolinium, terbium, dysprosium, erbium, lutetium) and their structural and vibrational properties. Polycrystalline powders were fabricated using a ball milling mechanochemical process, and their structural properties were assessed by X-ray diffraction (XRD) and transmission electron microscopy (TEM). The experimental lattice constants deduced from XRD and TEM were compared with density functional theory-based calculated lattice constants using the Perdew−Burke−Ernzerhof exchange-correlation functional. We show that the calculated lattice constants are within 1−1.5% of the experimental values for the majority of the *Ln*N species—a notable increase in accuracy over prior computational approaches. The frequencies of Raman scattering from the LO(Γ) phonon are reported across the series and compare well with published thin-film data on a smaller selection of the series. As expected, there is a linear relationship between the LO(Γ) phonon frequency and atomic number. Finally, we demonstrate that Raman spectroscopy can be used to detect the presence of a nanoscale oxide layer on the surface of ErN powders.

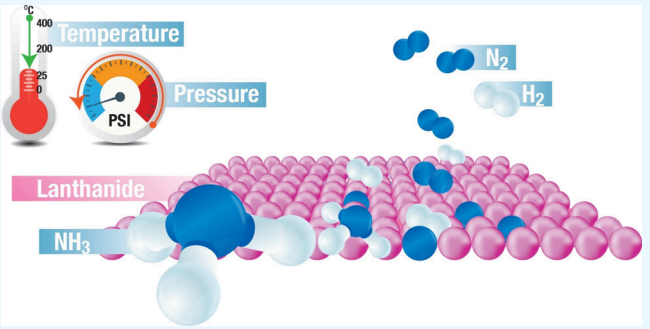

1. INTRODUCTION

The 14 lanthanide (*Ln*) elements from La to Lu are the only stable elements whose *f*-shells are filled to varying extents. They have been used in a large number of high-tech applications, such as wind turbines, electric vehicles, catalysis, consumer displays and lighting systems, and thus have been called *The Vitamins of Modern Industry*.[1] Their mononitrides, *Ln*N, are among their simplest compounds, adopting the FCC (NaCl) crystal structure. The semiconducting *Ln*N have seen a significantly strengthening interest in the past decade based largely on their intrinsic ferromagnetic ground state. They thus have inherent and unique complementary magnetic and electronic properties that make them attractive for spintronics activity.[2,3]

Previous studies have focused on thin films, the prototypical architecture of a spintronics device, but there is a growing interest in utilizing the *Ln*N in alternative forms (e.g., powders, pellets and bulk materials).[4−6] This is especially crucial in the development of new heterogeneous catalysts that contribute to the decarbonisation of ammonia production, one of the world's largest and most environmentally harmful chemical industries. Computational and theoretical works have highlighted that the promising new Mars-van Krevelen reaction mechanism utilizing metallic nitride catalysts,[7,8] including *Ln*N, could allow for a less energy-intensive ammonia synthesis with a lower carbon footprint.[9,10] However, much of the experimental research in this field, especially *Ln*N powder fabrication and characterization, is in its infancy. The propensity of *Ln*N to decompose in air forming oxide and hydroxides has prevented in-depth characterization and led to ambiguous conclusions.[4,6]

*Ln*N, whose NaCl crystal structure places all constituent ions at the centers of inversion symmetry, necessarily show no conventional 1-phonon Raman spectra.[11] Earlier Raman studies across the *Ln*N series showed a moderately strong and narrow line at a frequency in the 450−600 cm^{-1} range, depending on the lattice constant, which were suggested to be activated by nitrogen vacancies, a common defect in the *Ln*N.[12,13] Interestingly recent studies show no nitrogen vacancy dependence on the strength of the Raman signal.[14]

Received: September 26, 2024
Revised: November 4, 2024
Accepted: November 12, 2024
Published: November 18, 2024

The data are, however, similar to those reported many years ago on semiconductors with the NaCl crystal structure suggesting that it is an LO(Γ) vibration mediated by the Fröhlich interaction.[15] This proposal is strengthened by the appearance of Raman scattering at double the single LO(Γ) vibration frequency, a 2-phonon scattering that is a feature of the Fröhlich-interaction scenario. In the present manuscript, the *Ln*N powders we study show the clear 1-phonon scattering seen in thin films. However, 2-phonon scattering is weak at best in the poor signal-to-noise ratio common for Raman scattering from powder samples.[16]

*Ln*N have a propensity to react rapidly with oxygen and moisture when exposed to air under ambient conditions. The previous thin films used for Raman studies offer a relatively easily- established crystalline structure and, if they are adequately passivated, little opportunity for oxidation. The geometry of the optical measurement can also be well controlled, making comparative scattering strength studies among various films relatively straightforward.[12,14,17] In contrast, particle size distribution and compactness are known to have significant confounding effects on Raman signals of powders and are less controllable with regards to the optical geometry used in the measurements.[16] While this is measured clearly by a weaker intensity signal on our powder samples, we show in this report good correspondence when compared with previously reported experimental values for thin films, both in terms of phonon frequencies and signal width.

In this study, we report on the synthesis of nine *Ln*N powders (*Ln* = La, Ce, Nd, Sm, Gd, Tb, Dy, Er, Lu) and their structural/compositional characterization, followed by the results from Raman spectroscopy—the most extensive study on *Ln*N powders to date. It is important to note that during the fabrication and characterization measurements presented in this report, the *Ln*N powders were never exposed to air. Cryogenic transmission electron microscopy (TEM), X-ray diffraction analysis (XRD) and Raman spectroscopy were applied using airtight sample holders to prevent any air contamination—no passivating layer was used on the surface of the *Ln*N powders. We furthermore extend the study to ErN powders that have undergone controlled partial oxidation. Raman measurements undoubtedly show the presence of both nitride and oxide forms in the partially oxidized powders, supporting the core/shell-like structure observed by cryogenic transmission electron microscopy. The conclusions include the confirmation of the 1-phonon frequency for *Ln*N in polycrystalline powders and the ability of Raman spectroscopy to identify a thin oxide layer of a few atomic layers on top of the *Ln*N powders.

2. RESULTS AND DISCUSSION

The high energy ball milling technique has been used to synthesize *Ln*N powders. Lanthanum (La), cerium (Ce), neodymium (Nd), samarium (Sm), gadolinium (Gd), terbium (Tb), dysprosium (Dy), erbium (Er) and lutetium (Lu) metallic fillings were used as feedstock in the ball mill for nitridation and size reduction inside a nitrogen glovebox. The initial conditions for milling were chosen based on a literature review of the nitridation of dysprosium and cerium during ball milling and were adapted to make the process as efficient as possible.[6] Throughout the milling process, in a nitrogen glovebox, as the *Ln* metallic filings deform and reduce in size the new surfaces are exposed to N_2 in the jar forming *Ln*N powders due to the facile breaking of molecular nitrogen by *Ln* metallic surfaces.[9,10,18] The ball milling process results in particle size distribution of the *Ln*N powder of 10 μm. GdN and LuN thin films (100 nm thick) were used for comparison. Details on the growth of those films can be found elsewhere.[15]

The XRD diffractograms of *Ln*N powders are shown in Figure 1. The powders are polycrystalline with only peaks

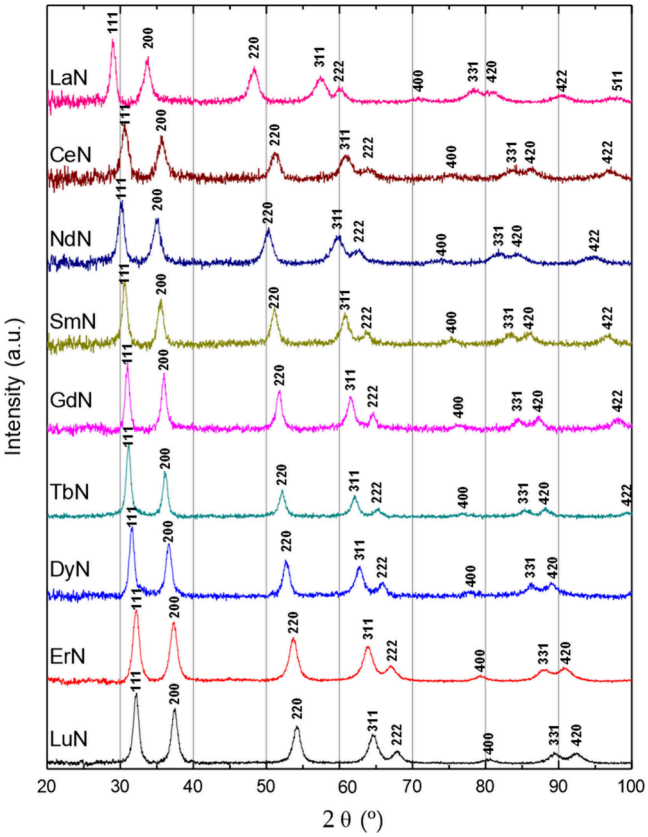

Figure 1. XRD patterns of *Ln*N powders (*Ln* = La, Ce, Nd, Sm, Gd, Tb, Dy, Er, Lu) with Miller indices labeled.

corresponding to the *Ln*N rock salt structure visible—no strong signals from pure lanthanide metal or oxide phases are observed. The relative peak intensities for all of the XRD diffractograms agree with the expected peak intensities for randomly oriented powder samples. The XRD data are also consistent with high-quality polycrystalline *Ln*N thin films grown in ultrahigh vacuum systems.[2] The average crystallite size was calculated for all samples, from the 111, 200, and 220 peaks, as these are the dominant peaks in all samples, returning an average crystallite size ranging from 10 to 15 nm. The deduced lattice constants (Figure 2), which decrease with increasing 4*f* band occupancy of the lanthanide atoms, are expected from the decrease of cation sizes across the lanthanide series. The lattice parameters suggest near stochiometric *Ln*N powders with limited nitrogen vacancies, at least for SmN, GdN and DyN.[14,19]

Lattice constants calculated for stoichioemetric *Ln*N using density functional theory are also presented in Figure 2, as well as experimental values from the literature.[2] Lattice constant calculations were performed using density functional theory as implemented in the Vienna *ab initio* Simulation Package (VASP).[20,21] The PBE exchange-correlation functional was used, and the valence electrons were represented using a plane

https://doi.org/10.1021/acsomega.4c08638
ACS Omega 2024, 9, 47842−47847

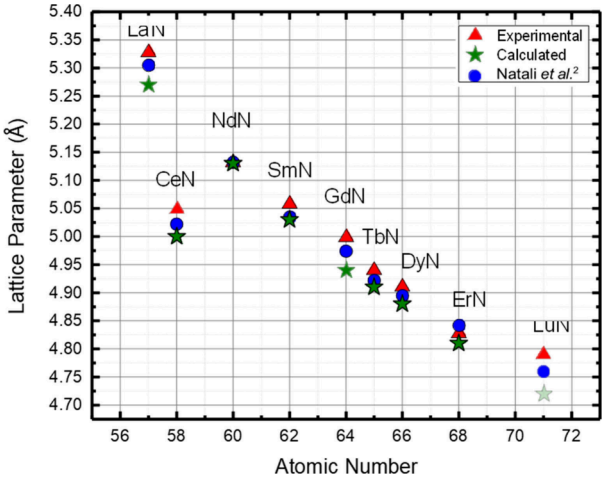

Figure 2. Lattice constants of *Ln*N powders versus atomic number alongside calculated lattice constants using the PBE exchange-correlation functional and previously reported experimental values for thin films and bulks from F. Natali et al.[2]

wave basis set with an energy cutoff of 400 eV.[22] The core electrons were represented using the projector-augmented wave method.[23] For N, La, and Ce, regular projector-augmented wave potentials were used, while for the rest of the rare earth species, we chose to use the projector-augmented wave potential which keeps the 4*f* electrons frozen in the core. This fixes the formal valency of these rare earth species to 3. A Monkhorst−Pack k-point sampling of 8 × 8 × 8 was used for all calculations. The self-consistent electron density was determined by iterative diagonalization of the Kohn−Sham Hamiltonian, with the Kohn−Sham states smeared according to a Fermi−Dirac distribution with a smearing parameter of k_BT = 0.1 eV, and energies extrapolated to σ = 0. The van der Waals interactions were described using the D3 scheme.[24] Optimal lattice constants were found by calculating the total energy of a series of systems with changing lattice constants and taking the lattice constant that gives the minimum total energy. The calculated lattice constants are within 1−1.5% of the experimental values for the majority of the *Ln*N species. This is a notable increase in accuracy over prior calculated values, where the LSDA+U method overestimated lattice constants by around 1 to 3%[25] and an all-electron method underestimated lattice constants by around 5 to 7%.[26] This suggests that using the *f*-in-core potentials approach to calculating *Ln*N systems may have great utility for describing their structure.

Raman spectroscopy was performed at ambient temperatures using a Jobin-Yvon LabRam HR employing laser excitation wavelengths of 457, 514.5, and 633 nm. All spectra were taken with 1 mW power to limit heating the powder under the laser illumination. The spectral resolution was ∼1 cm^{-1}, significantly finer than the spectral features being investigated. Figure 3 shows the main Raman peaks for the *Ln*N powders studied, omitting the CeN data which were too weak to resolve clearly. Note that the data in Figure 3 have been normalized to range from zero to one. They show remarkable concordance with data on thin films, clearly indicating that the powders comprise predominantly *Ln*N. As expected we see a clear shift in the phonon frequency across the series.[12] There is also a noticeable difference in signal-to-noise ratio and peak intensity but no clear pattern except to

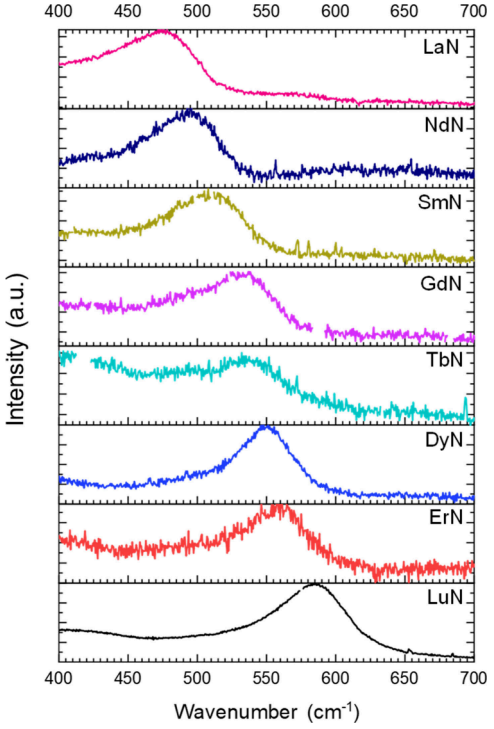

Figure 3. Raman spectra of *Ln*N powders (*Ln* La, Nd, Sm, Gd, Tb, Dy, Er, Lu) excited at 514.5 nm.

note that LaN (empty 4*f* shell) and LuN (full 4*f* shell) have the strongest peaks and largest signal-to-noise ratio. It is also important to note that the peak width and position were similar for all three excitation wavelengths, and while the background intensity differs, the *Ln*N peak is of similar absolute intensity for all three excitation wavelengths (not shown). The LO(Γ) frequency implied by the results is shown in Figure 4(a) as a function of the atomic number, compared with thin-film data.[12] In agreement with those data, there is a linear relationship between phonon frequency and atomic number and an inverse relationship with lattice constant.[12] The 1-phonon frequency and peak width were calculated assuming a linear background in several sample locations and averaged over all three excitation wavelengths. We report the following 1-phonon frequencies for the first time: LaN (473 ± 4 cm^{-1}), NdN (494 ± 8 cm^{-1}), and TbN (537 ± 8 cm^{-1}). Although the intensity of the peak varies greatly, the width is similar across the series (not shown). Again there is surprisingly good correspondence when compared with thin films.[12,15]

Clear two-LO(Γ) scattering has been reported in thin films.[12,15,17] Among our powders it is only ErN and LuN that show such a 2LO(Γ) feature, as seen in Figure 4(b). GdN, TbN, and DyN powders do not have clearly resolved higher frequency features. Interestingly, the three lightest *Ln*N for which we have data (LaN, NdN, and SmN) do not show a 2LO(Γ) peak but surprisingly do have prominent peaks (see Figure 4(b)) at a frequency ∼190 cm^{-1} higher. Suggestively, data from GdN and LuN thin films that have been grown in activated nitrogen from a Kaufman ion source show a similar peak above 2LO(Γ)—peak frequencies that have also been plotted in Figure 4(b). These features are likely related to defects introduced by the ions from the Kaufman source, though we currently have no good model to explain their physical origin.

https://doi.org/10.1021/acsomega.4c08638
ACS Omega 2024, 9, 47842−47847

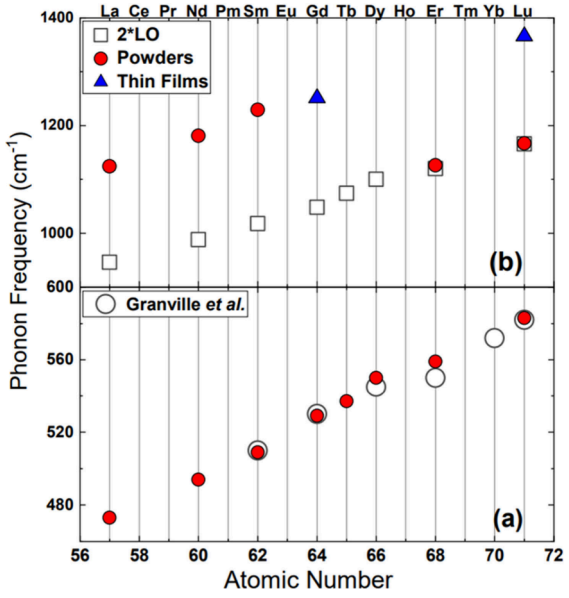

Figure 4. (a) Lo(Γ) frequencies for *Ln*N powders with previously reported experimental values for thin films reported by S. Granville et al.[10] versus atomic number. (b) Higher phonon frequencies versus atomic number compared with both 2LO(Γ) from our data and thin film data from K. Van Koughnet et al.[16]

The above presented evidence all indicate that the powders studied contain particles of *Ln*N. In order to investigate the feasibility of using Raman spectroscopy to detect small changes to the surface of the powders, Raman spectra of ErN powders were compared to partially oxidized ErN (PO-ErN) powders in Figure 5. In the PO-ErN spectra we see the ErN peak is

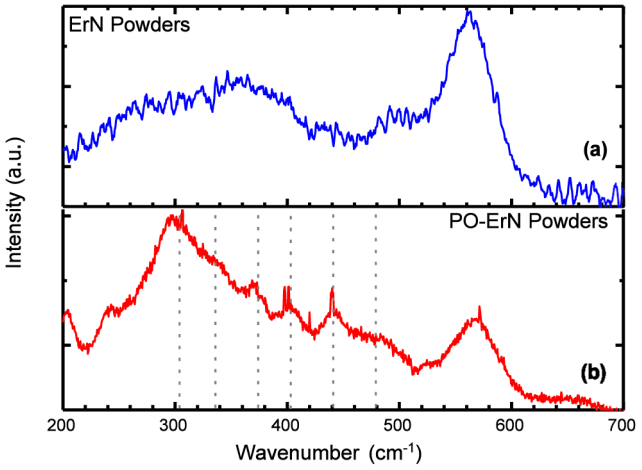

Figure 5. (a) Raman spectrum of ErN powders and (b) partially oxidized ErN (PO-ErN) excited at 514.5 nm. The vertical dashed lines correspond to reported Er_2O_3 lines by N. Dilawar et al.[27]

present along with a number of other features similar to previously reported phonon frequencies (vertical lines) for Er_2O_3.[27] Vibrational bands for lanthanide oxides tend to be significantly stronger than those reported for nitrides, so the dwarfing of the ErN peak by the Er_2O_3 peaks is expected. However, in the partially oxidized sample there is still significantly more nitride than oxide resulting in the nitride peak still being visible. The differences seen between the spectra in Figure 5 indicate that Raman spectroscopy detected evidence of the thin layer of oxidization. This is in direct contrast to XRD data for partially oxidized ErN, which only showed evidence of the nitride but is in good agreement with cryogenic TEM that shows the presence of a very thin Er_2O_3 oxide layer (see below). All the *Ln*N powders showed a broad and weak feature between 200−450 cm^{-1} that was present with all three excitation wavelengths. We believe that this might be due to the presence of small residual contamination.

Figure 6 shows a high-resolution TEM image of ErN powders. The lattice fringes in the interior of the particle have

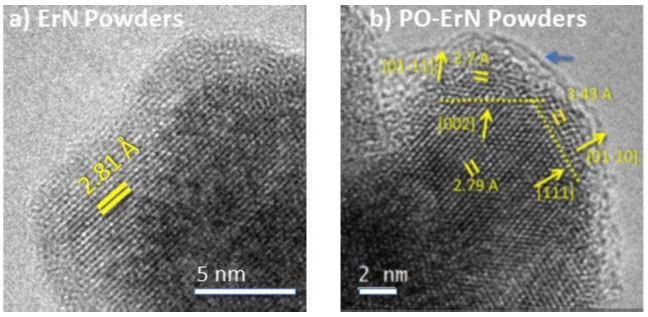

Figure 6. (a) HRTEM image of ErN particles showing lattice fringe spacing of 2.81 Å, corresponding to the FCC d_{111} lattice plane of ErN. (b) HRTEM of a partially oxidized ErN particle, showing a core (ErN)−shell (Er_2O_3) structure.

a lattice spacing of 2.81 Å corresponding to the FCC d_{111} lattice plane of ErN. The ErN nature of the powder is also confirmed by the spatial frequencies determined from a fast Fourier transform (FFT) (not shown), returning a lattice constant of $a = 4.85 \pm 0.06$ Å. This is within the experimental error margin of the expected lattice constant for FCC ErN in the literature and is similar to the lattice parameters inferred from XRD on the ErN powders (see Figure 1). In contrast, the high-resolution TEM of partially oxidized ErN shows a different structure in Figure 6. The dashed lines indicate the boundary between a core and a shell. One boundary is on the 111 plane, and the other is on the 002 plane. Considering first the 111 facet, the planes in the shell have a spacing of 3.43 Å which corresponds to the Er_2O_3 d_{01-10} lattice plane indicating an orientation relationship of 111//01−10. For the shell boundary on the cubic 002 plane, the shell has an observed lattice constant of 2.7 Å which corresponds to the Er_2O_3 d_{01-11} plane.

3. CONCLUSION

In conclusion, nine lanthanide nitride powders were synthesized using ball milling and investigated by XRD, TEM, and Raman spectroscopy. Three 1-phonon frequencies of *Ln*N are reported for the first time, and five are compared with previously reported results for thin films confirming remarkable similarity despite their uncontrolled geometry. We show that there is a directly proportional relationship between the LO(Γ) phonon (1-phonon), frequency, and atomic number and an inversely proportional relationship with lattice constant governed by the inverse square of the Ln−N bond length. The two heaviest *Ln*N (ErN and LuN) show a single 2-phonon peak at twice the frequency of the 1-phonon peak. Interestingly, some *Ln*N do not show a 2-phonon peak but have a prominent peak at a higher frequency (~190 cm^{-1} higher than twice the 1-phonon peak) that can also be seen in thin films—its origin is still puzzling. Finally, as a case study,

https://doi.org/10.1021/acsomega.4c08638
ACS Omega 2024, 9, 47842−47847

partially oxidized and unoxidized erbium nitride powders were compared. While XRD detected no difference in the samples, Raman spectra and TEM consistently revealed strong evidence of a thin surface layer of erbium oxide in the partially oxidized sample, highlighting the powerful sensitivity of Raman spectroscopy to detect small concentrations and fine surface structure. Our results underscore that high quality powders of lanthanide nitride can be obtained by a simple mechanical synthesis route, opening a new range of potential applications for these materials, including green ammonia synthesis.

AUTHOR INFORMATION

Corresponding Authors

Franck Natali − *The MacDiarmid Institute for Advanced Materials and Nanotechnology, School of Chemical and Physical Sciences, Victoria University of Wellington, Wellington 6140, New Zealand; Liquium Ltd., Laby Building, Victoria University of Wellington, Wellington 6012, New Zealand;* orcid.org/0000-0001-5407-1929; Email: franck.natali@vuw.ac.nz

Kiersten Kneisel − *The MacDiarmid Institute for Advanced Materials and Nanotechnology, School of Chemical and Physical Sciences, Victoria University of Wellington, Wellington 6140, New Zealand*; Email: kiersten.kneisel@vuw.ac.nz

Authors

Mohsen Maddah − *Liquium Ltd., Laby Building, Victoria University of Wellington, Wellington 6012, New Zealand*

Jay Chan − *Liquium Ltd., Laby Building, Victoria University of Wellington, Wellington 6012, New Zealand*

Ying Xu − *Liquium Ltd., Laby Building, Victoria University of Wellington, Wellington 6012, New Zealand*

Caitlin Casey-Stevens − *The MacDiarmid Institute for Advanced Materials and Nanotechnology, School of Chemical and Physical Sciences, Victoria University of Wellington, Wellington 6140, New Zealand*

Kiri Van Koughnet − *The MacDiarmid Institute for Advanced Materials and Nanotechnology, School of Chemical and Physical Sciences, Victoria University of Wellington, Wellington 6140, New Zealand*

William Holmes-Hewett − *The MacDiarmid Institute for Advanced Materials and Nanotechnology, Robinson Research Institute, Victoria University of Wellington, Wellington 6140, New Zealand*

Harry Joseph Trodahl − *School of Chemical and Physical Sciences, Victoria University of Wellington, Wellington 6140, New Zealand*

Complete contact information is available at: https://pubs.acs.org/10.1021/acsomega.4c08638

Notes

The authors declare no competing financial interest.

ACKNOWLEDGMENTS

We acknowledge funding and support from the MacDiarmid Institute for Advanced Materials and Nanotechnology, funded by the New Zealand Centres of Research Excellence Fund.

REFERENCES

(1) Spellman, F. R. *The Science of Rare Earth Elements: Concepts and Applications*, 1st ed.; CRC Press: Boca Raton, 2022.

(2) Natali, F.; Ruck, B. J.; Plank, N. O. V.; Trodahl, H. J.; Granville, S.; Meyer, C.; Lambrecht, W. R. L. Rare-earth mononitrides. *Prog. Mater. Sci.* **2013**, *58*, 1316−1360.

(3) Aerts, C.; Strange, P.; Horne, M.; Temmerman, W.; Szotek, Z.; Svane, A. Half-metallic to insulating behavior of rare-earth nitrides. *Phys. Rev. B* **2004**, *69*, No. 045115.

(4) Butt, D. P.; Jaques, B. J.; Osterberg, D. D.; Marx, B. M.; Callahan, P. G.; Hamdy, A. S. New routes to lanthanide and actinide nitrides. *Proceedings of Global 2009: The Nuclear Fuel Cycle: Sustainable Options & Industrial Perspectives*; 2009; p 9057.

(5) Takano, M.; Itoh, A.; Akabori, M.; Minato, K. *Hydrolysis reactions of rare-earth and americium mononitrides J. Phys. Chem. Solids* **2005**, *66*, 697.

(6) Jaques, B. J.; Osterberg, D. D.; Alanko, G. A.; Tamrakar, S.; Smith, C. R.; Hurley, M. F.; Butt, D. P. *In situ* characterization of the nitridation of dysprosium during mechanochemical processing. *J. Alloys Comp.* **2015**, *619*, 253−261.

(7) Ye, T.-N; Park, S.-W.; Lu, Y.; Li, J.; Sasase, M.; Kitano, M.; Hosono, H. Contribution of Nitrogen Vacancies to Ammonia Synthesis over Metal Nitride Catalysts. *J. Am. Chem. Soc.* **2020**, *142* (33), 14374−14383.

(8) Daisley, A.; Hargreaves, J. S. Metal nitrides, the Mars-van Krevelen mechanism and heterogeneously catalysed ammonia synthesis Catal. *Today* **2023**, *423*, 113874.

(9) Ullstad, F.; Bioletti, G.; Chan, J. R.; Proust, A.; Bodin, C.; Ruck, B. J.; Trodahl, H. J.; Natali, F. Breaking Molecular Nitrogen under Mild Conditions with an Atomically Clean Lanthanide Surface. *ACS Omega* **2019**, *4*, 5950−5954.

(10) Chan, J. R.; Lambie, S. G.; Trodahl, H. J.; Lefebvre, D.; Le Ster, M.; Shaib, A.; Ullstad, F.; Brown, S. A.; Ruck, B. J.; Garden, A. L.; Natali, F. Facile dissociation of molecular nitrogen using lanthanide surfaces: Towards ambient temperature ammonia synthesis. *Phys. Rev. Mater.* **2020**, *4*, 115003.

(11) Cardona, M. Light Scattering in Solids I: Introductory Concepts. *In Vol. 8 of Topics in Applied Physics*, 2nd ed.; Springer: Berlin Heidelberg, 2005.

(12) Granville, S.; Meyer, C.; Preston, A.; Ludbrook, B.; Ruck, B.; Trodahl, H.; Paudel, T.; Lambrecht, W. Vibrational properties of rare-earth nitrides: Raman spectra and theory. *Phys. Rev. B* **2009**, *79*, No. 054301.

(13) Upadhya, K.; Kumar, R.; Li, Q.; Sun, B.; Saha, B. Vibrational Spectrum and Thermal Conductivity of Rare-Earth Semiconducting Erbium Nitride Thin Films. *Phys. Status Solidi RRL* **2022**, *16*, 2200029.

(14) Shaib, A.; Natali, F.; Chan, J. R.; Ullstad, F.; Holmes-Hewett, W. F.; Miller, J. D.; Ruck, B. J.; Trodahl, H. J. Coexisting structural phases in the catalytically driven growth of rock salt GdN *Mater. Res. Express* **2020**, *7*, No. 046404.

(15) Van Koughnet, K.; Trodahl, H.; Holmes-Hewett, W.; Ruck, B. Defect-activated versus intrinsic Raman spectra of GdN and LuN. *Phys. Rev. B* **2023**, *108*, No. 064306.

(16) Chen, Z.-P.; Li, L.-M.; Jin, J.-W.; Nordon, A.; Littlejohn, D.; Yang, J.; Zhang, J.; Yu, R.-Q. Quantitative analysis of powder mixtures by Raman spectrometry: the influence of particle size and its correction. *Anal. Chem.* **2012**, *84*, 4088.

(17) Al Atabi, H. A.; Al Auda, Z. F.; Padavala, B.; Craig, M.; Hohn, K.; Edgar, J. H. Sublimation growth and characterization of erbium nitride crystals. *Cryst. Growth Des.* **2018**, *18*, 3762.

(18) Chan, J. R.; Casey-Stevens, C. A.; Le Ster, M.; Shaib, A.; Tadich, A.; Cowie, B. C. C.; Trodahl, H. J.; Brown, S. A.; Granville, S.; Ruck, B. J.; Garden, A. L.; Natali, F. Epitaxial growth of gadolinium and samarium thin films and their subsequent facile nitridation at ambient temperatures. *Appl. Surf. Sci.* **2023**, *632*, 157550.

(19) Shaib, A.; Natali, F.; Chan, J. R; Ullstad, F.; Holmes-Hewett, W. F; Miller, J. D; Ruck, B. J; Trodahl, H. J Coexisting structural phases in the catalytically driven growth of rock salt GdN. *Mater. Res. Express* **2020**, *7*, 046404.

https://doi.org/10.1021/acsomega.4c08638
ACS Omega 2024, 9, 47842−47847

(20) Kresse, G.; Furthmüller, J. Efficient iterative schemes for ab initio total-energy calculations using a plane-wave basis set. *Phys. Rev. B* **1996**, *54*, 11169.
(21) Kresse, G.; Joubert, D. From ultrasoft pseudopotentials to the projector augmented-wave method. *Phys. Rev. B* **1999**, *59*, 1758.
(22) Perdew, J. P.; Burke, K.; Ernzerhof, M. Generalized Gradient Approximation Made Simple. *Phys. Rev. Lett.* **1996**, *77*, 3865.
(23) Blöchl, P. E. Projector augmented-wave method. *Phys. Rev. B* **1994**, *50*, 17953.
(24) Grimme, S.; Antony, J.; Ehrlich, S.; Krieg, H. A consistent and accurate ab initio parametrization of density functional dispersion correction (DFT-D) for the 94 elements H-Pu. *J. Chem. Phys.* **2010**, *132*, 154104.
(25) Larson, P.; Lambrecht, W. R. L.; Chantis, A.; van Schilfgaarde, M. Electronic structure of rare-earth nitrides using the LSDA+*U* approach: Importance of allowing 4*f* orbitals to break the cubic crystal symmetry. *Phys. Rev. B* **2007**, *75*, No. 045114.
(26) Topsakal, M.; Wentzcovitch, R. Accurate projected augmented wave (PAW) datasets for rare-earth elements (RE = La−Lu). *Comput. Mater. Sci.* **2014**, *95* (2014), 263.
(27) Dilawar, N.; Mehrotra, S.; Varandani, D.; Kumaraswamy, B.; Haldar, S.; Bandyopadhyay, A. A Raman spectroscopic study of C-type rare earth sesquioxides. *Mater. Charact* **2008**, *59* (2008), 462.

https://doi.org/10.1021/acsomega.4c08638
ACS Omega 2024, 9, 47842−47847